

Invariant Tensor Feature Coding

Yusuke Mukuta

The University of Tokyo, RIKEN AIP

mukuta@mi.t.u-tokyo.ac.jp

Tatsuya Harada

The University of Tokyo, RIKEN AIP

harada@mi.t.u-tokyo.ac.jp

Abstract

We propose a novel feature coding method that exploits invariance. We consider the setting where the transformations that preserve the image contents compose a finite group of orthogonal matrices. This is the case in many image transformations, such as image rotations and image flipping. We prove that the group-invariant feature vector contains sufficient discriminative information when learning a linear classifier using convex loss minimization. From this result, we propose a novel feature modeling for principal component analysis and k -means clustering, which are used for most feature coding methods, and global feature functions that explicitly consider the group action. Although the global feature functions are complex nonlinear functions in general, we can calculate the group action on this space easily by constructing the functions as the tensor product representations of basic representations, resulting in the explicit form of invariant feature functions. We demonstrate the effectiveness of our methods on several image datasets.

1. Introduction

Feature coding is the method that calculates one global feature by summarizing the statistics of local features extracted from one image. To obtain the local features $\{x_n\}_{n=1}^N \in \mathbb{R}^{d_{\text{local}}}$, we use a nonlinear function F and $F = \frac{1}{N} \sum_{n=1}^N F(x_n) \in \mathbb{R}^{d_{\text{global}}}$ as a global feature. Currently, we use activations of convolutional layers of pre-trained CNNs such as VGG-Net [33] as local features to obtain considerable performance improvement [31, 37]. Further, existing works handle coding methods as differentiable layers and train them end-to-end to obtain high accuracy [2, 10, 22]. Thus, feature coding is a general method for transferring the information of CNNs to a wider domain.

The invariance of images under geometric transformations is essential for image recognition because we can obtain compact and discriminative features by focusing on the information invariant to the transformations that preserve image contents. For example, some researchers construct

CNNs with more complex invariances, such as image rotation [4, 5, 40], and obtain a model with high accuracy with reduced model parameters. Therefore, we expect to construct a feature coding method that contains highly discriminative information per dimension and is robust to the considered transformations by exploiting invariance information in the coding methods.

In this work, we propose a novel feature coding method that exploits invariance. Specifically, we assume that the transformations \mathcal{T} that preserve the image contents act as a finite group consisting of orthogonal matrices on each local feature x_n . For example, when we use the concatenation of pixel values in the image subregion as the local feature, image flipping acts as the change of pixel values. Hence, it can be represented by a permutation matrix, which is orthogonal. We ignore the change in the feature position because we apply global feature pooling. We need to construct a nonlinear feature coding function F that exploits \mathcal{T} . Our first result is that when we learn the linear classifier using l_2 -regularized convex loss minimization on the vector space where \mathcal{T} act as orthogonal matrices, the learned weight exists in the subspace invariant under the \mathcal{T} action. From this result, we propose a guideline that we first construct a vector space in which \mathcal{T} act orthogonally on $F(x_n)$, and calculate the \mathcal{T} -invariant subspace.

Two problems occur in constructing the global feature. The first problem is that, in general, F exhibits complex nonlinearity. The action of \mathcal{T} on CNN features can be calculated relatively easily because CNNs consist of linear transformations and point-wise activation functions. This is not the case for feature coding methods. The second is that we must learn F from the training data. When we encode the feature, we first apply principal component analysis (PCA) on x_n to reduce the dimension. We often learn the clustering using k -means or Gaussian Mixture Model (GMM) and calculate F from the learned model. Therefore, we must consider the effect of \mathcal{T} on the learned model.

To solve these problems, we exploit two concepts of group representation theory: reducible decomposition of the representation and tensor product of two representations. The former is the decomposition of the action of \mathcal{T} on

x_n into the direct sum of irreducible representations. This decomposition is important when we construct the dimensionality reduction method that is compatible with group action, and we subsequently calculate the tensor product of the representations. The tensor product of the representations is the method by which we construct a vector space where the group acts from the product of input representations. Therefore, it is important when we construct nonlinear feature functions that the group action can be easily calculated.

With these concepts, we propose a novel feature coding method and model training methods that exploit the group structure. We applied our methods to the D4 group that consists of $\pi/2$ rotations and flipping and conducted experiments on image recognition datasets. We observed the performance improvement and robustness to such image transformations.

In summary, our contributions are as follows:

- We prove that the linear classifier becomes group-invariant when trained on the space where the group of content-preserving transformations acts orthogonally.
- We propose a group-invariant extension of feature modeling and feature coding methods when the group acts orthogonally on local features.
- We evaluated the accuracy and invariance of our methods on image recognition datasets.

2. Related Work

2.1. Feature coding

Two types of feature coding approaches exist: covariance-based and clustering-based approaches.

The covariance-based approach models the distributions of local features using Gaussian distributions and uses statistics as the global feature. For example, GLC [26] uses the mean and covariance of the local descriptors as the feature. The global Gaussian [27] applies an information-geometric metric on the statistical manifold of the Gaussian distribution as the similarity measure. Bilinear pooling (BP) [22] uses the mean of self-products instead of the mean and covariance, but the performance is similar. BP is defined as $F = \text{vec} \left(\frac{1}{N} \sum_{n=1}^N x_n x_n^t \right)$, where $\text{vec}(A)$ denotes the vector that stores the elements of A . Because of the simplicity of BP, there are various extensions, such as [21, 36, 11]. For example, improved bilinear pooling (iBP) uses the matrix square root as a global feature.

The most simple clustering-based approach is the vector of locally aggregated descriptors (VLAD) [14]. The VLAD is a Cd_{local} -dimensional vector that uses k-means clustering, where C is the number of clustering components, and consists of the sum of the differences from each local feature to the cluster centroid μ_c to which it is assigned, writ-

ten as $F_c = \sum_{x_n \in S_c} (x_n - \mu_c)$, where S_c is the set of local descriptors that are assigned to the c -th cluster. The vector of locally aggregated tensors (VLAT) [28] is an extension of the VLAD that exploits second-order information. The VLAT uses the sum of tensor products of the differences from each local descriptor to the cluster centroid μ_c : $F_c = \text{vec} \left(\sum_{x_n \in S_c} (x_n - \mu_c)(x_n - \mu_c)^t - \mathcal{T}_c \right)$, where \mathcal{T}_c is the mean of $(x_n - \mu_c)(x_n - \mu_c)^t$ of all the local descriptors assigned to the c -th cluster. The VLAT contains information similar to the full covariance of the GMM. The Fisher vector (FV) [31] also exploits second-order information but uses only diagonal covariance. There also exists work that exploits local second order information with lower feature dimension using local subspace clustering [7].

2.2. Feature extraction that considers invariance

One direction for exploiting the invariance in model structure is to calculate all the transformations and subsequently apply pooling with respect to the transformation to obtain the invariant feature. TI-Pooling [18] first applies various transformations on input images, subsequently applies the CNN with the same weight, and finally applies max-pooling to obtain the invariant feature. Anselmi et al. [1] also proposed a layer that averages the activations with respect to all the considered transformations. RotEqNet [24] calculates the vector field by rotating the convolutional filters and lines up with the activations, and subsequently applies pooling to the vector fields to obtain rotation-invariant features. Group equivariant CNNs [4] construct a network by the average of activations with respect to the transformed convolutional filters and point-wise activations.

Another direction is to exploit the group structure of transformations and construct the feature using group representations. Harmonic networks [40] consider the continuous image rotation and construct a layer with spherical harmonics that is the basis of the representation of two-dimensional rotation groups. Steerable CNNs [4] consider the D4 group and construct the filter with the direct sum of the irreducible representations of the group to reduce the model parameters while preserving accuracy. Weiler et al. [38] implemented steerable CNNs as the weighted sum of predefined equivariant filters and extended it to finer rotation equivariance. While these works mainly focus on equivariant convolutional layers, we mainly focus on invariant feature coding given equivariant local features. The difficulty of invariant feature coding is to formulate complex nonlinear feature coding functions that are consistent with considered transformations.

Another direction similar to our approach is to calculate the nonlinear invariance with respect to the transformations. Reiser & Burkhardt [29] considered 3D rotation invariance and used the coefficients with respect to spherical harmon-

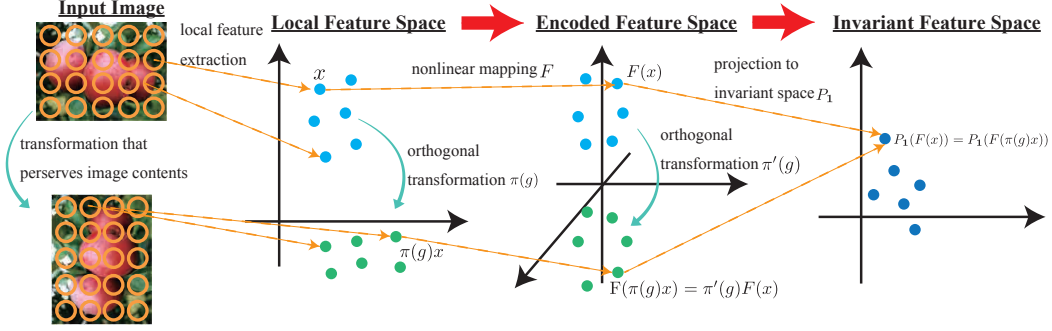


Figure 1. Overview of the proposed feature coding method. First, we construct a global feature space where $\pi'(g)F(x) = F(\pi(g)x)$ holds for some orthogonal π' . We subsequently apply the projection to the trivial representation to P_1 to obtain the invariant global feature.

ics as the invariant feature. Kobayashi et al. [16] calculated a rotation-invariant feature using the norm of the Fourier coefficients. Morère et al. [25] proposed group-invariant statistics by integrating all the considered transformations like Eq. (1) for image retrieval, though they do not assume the transformations act linearly. Kobayashi [15] exploited the fact that the eigenvalues of the representation of flipping are ± 1 and used the absolute values of coefficients of eigenvectors as the feature. Ryu et al. [30] used the magnitude of two-dimensional discrete Fourier transformations as the translation-invariant global feature. Compared to these approaches, the advantages of our method are that although they heuristically calculate the invariants, we can algorithmically calculate the invariants given the transformations, and we can calculate all the invariants once we construct the vector space that the group acts on. Therefore, our method exhibits both versatility and high classification performance.

In summary, our work is an extension of existing coding methods where we can easily calculate the effect of transformations and all the invariants. Compared to existing invariant feature learning methods, we mainly focus on invariant feature coding from the viewpoint of group representation theory.

3. Overview of Group Representation Theory

In this section, we present an overview of the group representation theory necessary for constructing our method. We write these explanations for the self-completeness of the paper. The contents in this section are not original and written in most books about group representation, such as [9].

For readability, we summarize the essential points in this section for our methods beforehand as follows:

- Group representation is the homomorphism from the considered group to the matrix group.
- Group representation can be decomposed by the direct sum of irreducible representations.
- We can obtain all the invariant vectors by extracting the subspace with respect to the trivial representation

$\mathbf{1}$, which can also be obtained by Eq. (1).

- The linear operator that commutes with group action is restricted to the direct sum of linear operators between the same irreducible representations.
- We can obtain a nonlinear vector for the group that acts linearly by considering tensor product representation.

Group representation When set G and an operation $\circ : G \times G \rightarrow G$ satisfying the properties:

- \circ is associative: $g_1, g_2, g_3 \in G$ satisfies $((g_1 \circ g_2) \circ g_3) = (g_1 \circ (g_2 \circ g_3))$.
- The identity element $e \in G$ exists that satisfies $g \circ e = e \circ g = g$ for all $g \in G$.
- All $g \in G$ contains the inverse g^{-1} that satisfies $g \circ g^{-1} = g^{-1} \circ g = e$.

The pair $\mathcal{G} = (G, \circ)$ is called a group. The axioms above are the abstraction of the properties of the set of transformations. For example, the set consists of 2-D image rotations associated with the composition of transformations forms a group. When the number of elements in G written as $|G|$ is finite, \mathcal{G} is called a finite group. As mentioned in Section 1, we consider a finite group herein.

We now consider a complex vector space \mathbb{C}^d . We use a complex space for the simplicity of the theory; however, in our setting, the proposed global feature is real. The space of bijective on \mathbb{C}^d can be identified with the space of $d \times d$ regular complex matrices written as $GL(d, \mathbb{C})$, which is also a group with the matrix product as the operator. The homomorphism π from \mathcal{G} to $GL(d, \mathbb{C})$: the mapping $\pi : G \rightarrow GL(d, \mathbb{C})$ that satisfies

- For $g_1, g_2 \in G$, $\pi(g_1) \circ \pi(g_2) = \pi(g_1 \circ g_2)$.
- $\pi(e) = \mathbf{1}_{d \times d}$.

is called the representation of \mathcal{G} on \mathbb{C}^d , where $\mathbf{1}_{d \times d}$ denotes the d -dimensional identity matrix. When we explicitly denote the space that the matrices act on, we denote (π, \mathbb{C}^d) . The representation that maps all $g \in G$ to $\mathbf{1}_{d \times d}$ is called a trivial representation. We denote a one-dimensional trivial

representation as **1**. When all $\pi(g)$ are unitary matrices, the representation is called a unitary representation. Moreover, we call it an orthogonal representation when the $\pi(g)$ s are orthogonal matrices. An orthogonal representation is also a unitary representation. In this work, we assume that all transformations are orthogonal.

Intertwining operator For two representations (π, \mathbb{C}^d) , and $(\pi', \mathbb{C}^{d'})$, a linear operator $A : \mathbb{C}^d \rightarrow \mathbb{C}^{d'}$ is called an intertwining operator if it satisfies $\pi'(g) \circ A = A \circ \pi(g)$. This implies that $(\pi', A\mathbb{C}^d)$ also becomes a representation. Thus, when we apply linear dimension reduction, it is important that the projection matrix is an intertwining operator. We write the space of the intertwining operator as $\text{Hom}_G(\pi, \pi')$. When a bijective $A \in \text{Hom}_G(\pi, \pi')$ exists, we write $\pi \simeq \pi'$. This implies that the two representations are virtually the same, and that the only difference is the basis of the vector space.

Irreducible representation Given two representations π, σ , the mapping that associates g with the matrix that we concatenate $\pi(g), \sigma(g)$ in the block-diagonal form is the representation on the space of the direct sum of the input representation spaces. This representation is called the direct sum representation of π, σ , written as $\pi \oplus \sigma$. When the representation π is equivalent with some direct sum representations, π is called a completely reducible representation. The direct sum is the composition of space that the group acts on independently. Therefore, a completely reducible representation can be decomposed by independent and simpler representations. When the representation is unitary, the representation that cannot be decomposed is called an irreducible representation, and all representations are equivalent with the direct sum of irreducible representations. The irreducible representation τ_t s is decided from the group structure. π is decomposed by $\pi \simeq n_1\tau_1 \oplus n_2\tau_2 \oplus \dots \oplus n_T\tau_T$, where $n_t\tau_t$ is n_t times direct sum of τ_t . When we denote the characteristic function of g as $\chi_\pi(g) = \text{Tr}(\pi(g))$, we can calculate these coefficients as $n_t = \frac{1}{|G|} \sum_{g \in G} \chi_\pi(g) \chi_{\tau_t}(g)$. Further, the projection operator P_τ to $n_t\tau_t$ is calculated as $P_{\tau_t} = \dim(\tau_t) \frac{1}{|G|} \sum_{g \in G} \chi_{\tau_t}(g) \pi(g)$. Specifically, because $\chi_{\mathbf{1}}(g) = 1$, we can calculate the projection to the trivial representation using

$$P_{\mathbf{1}} = \frac{1}{|G|} \sum_{g \in G} \pi(g). \quad (1)$$

This equation reflects the fact that the average of all $\pi(g)$ is invariant to the group action. Schur's lemma indicates that $\text{Hom}_G(\tau_{t_1}, \tau_{t_2}) = \{0\}$ if $t_1 \neq t_2$ and $\text{Hom}_G(\tau_t, \tau_t) = \mathbb{C}A$ for some matrix A .

Tensor product representation Finally, we explain the tensor product representation. The tensor product representation is important when we construct nonlinear feature functions. Given π, σ , the mapping that associates g with the matrix tensor product of $\pi(g), \sigma(g)$ is the representation on the space of the tensor product of input spaces. We write the tensor product representation as $\pi \otimes \sigma$. The tensor product of the unitary representation is also unitary. The important properties of the tensor representation are (i) a distributive property where $(\pi_1 \oplus \pi_2) \otimes (\pi_3 \oplus \pi_4) = (\pi_1 \otimes \pi_3) \oplus (\pi_2 \otimes \pi_3) \oplus (\pi_1 \otimes \pi_4) \oplus (\pi_2 \otimes \pi_4)$, and (ii) $\chi_{\pi \otimes \sigma}(g) = \chi_\pi(g) \chi_\sigma(g)$. Thus, we can calculate the irreducible decomposition of tensor representations from that of irreducible representations.

4. Invariant Tensor Feature Coding

In this section, we explain the proposed method. Our goal is to construct an effective feature function $F = \frac{1}{N} \sum_{n=1}^N F(x_n)$ when the transformations that preserve the image contents act as the finite group of orthogonal matrices on x_n . Hence, we prove a theorem that reveals the condition of the invariant feature with sufficient discriminative information in Section 4.1. We subsequently explain the feature modeling method necessary for constructing the coding in Section 4.2. We describe our proposed invariant feature function in Section 4.3. We finally discuss the group and local features used in the experiment in Section 4.4.

4.1. Guideline for Invariant Features

First, to decide what an effective feature is, we prove the following theorem.

Theorem 1. *When we assume finite group \mathcal{G} acts as an orthogonal representation π on \mathbb{R}^d and preserves the distribution of the training data $\{(v_m, y_m)\}_{m=1}^M \in \mathbb{R}^d \times \mathcal{C}$, which implies that $\{(\pi(g)v_m, y_m)\}_{m=1}^M \in \mathbb{R}^d \times \mathcal{C}$ exhibits the same distribution as $\{(\pi(g)v_m, y_m)\}_{m=1}^M \in \mathbb{R}^d \times \mathcal{C}$ for any g , the solution of the l_2 -regularized convex loss minimization*

$$\arg \min_{w \in \mathbb{R}^d} \frac{\lambda}{2} \|w\|^2 + \frac{1}{M} \sum_{m=1}^M l(\langle w, x_m \rangle_{\mathbb{R}}, y_m) \quad (2)$$

is \mathcal{G} -invariant, implying that $\pi(g)w = w$ for any g and $P_{\mathbf{1}}w = w$.

The \mathcal{G} -invariance of the training data corresponds to the fact that g does not change the contents of the image. From another viewpoint, this corresponds to data augmentation that uses transformed images as additional training data.

Proof. Non-trivial unitary representation τ satisfies $\sum_{g \in G} \tau(g) = 0$. This is because if we assume $\sum_{g \in G} \tau(g) = A \neq 0$, there exists v that satisfies

$Av \neq 0$ and $\mathbb{C}Av$ is a one-dimensional \mathcal{G} -invariant subspace. It violates the irreducibility of π . Because (π, \mathbb{R}^d) is a unitary representation of \mathcal{G} , it is completely reducible. We write the $n_t \tau_t$ elements of w and v_m as $w^{(t)}, v_m^{(t)}$. It follows that $w = \sum_{t=1}^T w^{(t)}$, $v_m = \sum_{t=1}^T v_m^{(t)}$. Further, $w^{(t)}$ s and $x_i^{(t)}$ s are orthogonal for different t s. It follows that

$$\begin{aligned}
& \frac{1}{M} \sum_{m=1}^M l(\langle w, v_m \rangle_{\mathbb{R}}, y_m) \\
&= \frac{1}{M} \sum_{m=1}^M l \left(\operatorname{Re} \left(\sum_{t=1}^T \langle w^{(t)}, v_m^{(t)} \rangle_{\mathbb{C}} \right), y_m \right) \\
&= \frac{1}{M|G|} \sum_{m=1}^M \sum_{g \in G} l \left(\operatorname{Re} \left(\sum_{t=1}^T \langle w^{(t)}, \tau_t(g^{-1})v_m^{(t)} \rangle_{\mathbb{C}} \right), y_m \right) \\
&= \frac{1}{M|G|} \sum_{m=1}^M \sum_{g \in G} l \left(\operatorname{Re} \left(\sum_{t=1}^T \langle \tau_t(g)w^{(t)}, v_m^{(t)} \rangle_{\mathbb{C}} \right), y_m \right) \\
&\geq \frac{1}{M} \sum_{m=1}^M l \left(\sum_{t=1}^T \operatorname{Re} \left(\left\langle \frac{1}{|G|} \sum_{g \in G} \tau_t(g)w^{(t)}, v_m^{(t)} \right\rangle_{\mathbb{C}} \right), y_m \right) \\
&= \frac{1}{M} \sum_{m=1}^M l \left(\langle w^{(1)}, v_m^{(1)} \rangle_{\mathbb{R}}, y_m \right), \tag{3}
\end{aligned}$$

where Re implies the real part of a complex number; the first equation comes from the orthogonality of $w^{(t)}$ s and $v_m^{(t)}$ s; the second equation comes from the \mathcal{G} -invariance of the training data; the third comes from the unitarity of $\tau_t(g)$; the inequation comes from the convexity of l , additivity of Re , and the inner products; the final equality comes from the fact that the average of $\tau_t(g)$ equals 0 for non-trivial τ_t ; $w^{(1)}$ and $v_m^{(1)}$ are real vectors.

Combined with the fact that $\|w\|^2 \geq \|w^{(1)}\|^2$, the loss value of w is larger than the loss value of $w^{(1)}$. Therefore, the solution is \mathcal{G} -invariant. \square

This theorem indicates that we can reduce the complexity of the problem by considering the invariance. Because the generalization error increases with the complexity, this theorem explains one reason that invariance contributes to the good test performance. Sokolic et al. analyzed the generalization error in a similar setting using a covering number [34]. While this work calculated the upper bound of the complexity, we focus on the linear classifier and obtain the explicit complexity and the form of the learned classifier. Hence, our guideline is to **construct a global feature as an invariant vector in the vector space where the group acts orthogonally**.

4.2. Invariant feature modeling

We first construct a novel feature modeling method necessary for calculating the feature coding methods that con-

Algorithm 1 Calculation of Invariant PCA

Require: $\{x_n\}_{n=1}^N \in \mathbb{R}^d, \mathcal{G}, d_{\text{proj}}$

Ensure: $W \in \mathbb{R}^{d \times d_{\text{proj}}}$ which is intertwining and orthonormal

for $t = 1$ to T **do**

for $o_1, o_2 = 1$ to n_t **do**

$$\Sigma^{(t)}_{o_1, o_2} \leftarrow \frac{1}{N} \sum_{n=1}^N \left\langle x_n^{(t, o_1)} - \mu^{(t, o_1)}, x_n^{(t, o_2)} - \mu^{(t, o_2)} \right\rangle_{\mathbb{R}}$$

end for

$(\lambda_p^{(t)}, u_p^{(t)}) \leftarrow$ eigendecomposition of $\Sigma^{(t)}$.

end for

$W =$ empty matrix

while size of W is smaller than $d \times d_{\text{proj}}$ **do**

$W \leftarrow$ concatenation of W and $(u_p^{(t)} \otimes I_{d_{\tau_t}}) \circ P_{\tau_t}$ for non-used p, t with maximum $\lambda_p^{(t)} / d_{\tau_t}$

end while

sider group action.

Invariant PCA The original PCA is the solution of

$$\max_{W^t W = I} \operatorname{Tr} \left(W^t \frac{1}{N} \sum_{n=1}^N (x_n - \mu)(x_n - \mu)^t W \right), \tag{4}$$

where $\mu = \frac{1}{N} \sum_{n=1}^N x_n$. PCA attempts to maximize the sum of the variances of the projected vectors. The solution is the matrix where we line up the eigenvectors of $\frac{1}{N} \sum_{n=1}^N (x_n - \mu)(x_n - \mu)^t$ that correspond to the top eigenvectors.

In addition to the original constraint $W^t W = I$, we assume that W is an intertwining operator to the projected space, such that the projected space is also the representation space. From Schur's lemma described in Section 3, W that satisfies these conditions is the matrix that we line up the composition of P_{τ_t} and the dimensionality reduction within $n_t \tau_t$. Further, when we denote $n_t \tau_t = \bigoplus_{o=1}^{n_t} \tau_{t, o}$ and the $\tau_{t, o}$ -th element of x_n as $x_n^{(t, o)}$, the dimensionality reduction within $n_t \tau_t$ is in the form of $x_n^{(t)} \rightarrow \sum_{o=1}^{n_t} w^{(t, o)} x_n^{(t, o)}$ for $w^{(t, o)} \in \mathbb{C}$ because of Schur's lemma. Hence, our basic strategy is to first calculate $w^{(t, o)}$ s that maximize the variance with the orthonormality preserved, and subsequently choose t for larger variances per dimension. In fact, $w^{(t, o)}$ s can be calculated using PCA with the sum of covariances between each dimensional element of $x_n^{(t, o)}$ s.

Because the projected vector must be real, additional care is required when some elements of τ_t are complex. We describe the modification for this case in the supplementary materials. In our application, we use the D4 group in which all irreducible representations can be real; thus, we can use τ_t directly. The algorithm is written in Algorithm 1.

Algorithm 2 Calculation of Invariant k-means

Require: $\{x_n\}_{n=1}^N \in \mathbb{R}^d, \mathcal{G}, C$

Ensure: $\mu_{g,c}$ for $g \in G, c \in \{1, \dots, C\}$

randomly initialize $\mu_{e,c}$ for $c \in \{1, \dots, C\}$

for it = 1 to maxiter **do**

$\mu_{g,c} \leftarrow \pi(g)\mu_{e,c}$ for $g \in G, c \in \{1, \dots, C\}$

$S_{g,c} \leftarrow \{n | (g, c) = \arg \min_{(g,c)} \|x_n - \mu_{g,c}\|\}$

$\mu_{e,c} \leftarrow \frac{1}{\sum_{g \in G} |S_{g,c}|} \sum_{g \in G} \sum_{n \in S_{g,c}} \pi(g)^{-1} x_n$ for $c \in \{1, \dots, C\}$.

end for

Invariant k-means The original k-means is calculated as

$$\min_{\mu} \sum_{n=1}^N \min_{c=1}^C \|x_n - \mu_c\|^2. \quad (5)$$

To guarantee that \mathcal{G} acts orthogonally on the learned model, we simply hold the cluster centroids by applying all the transformations to the original centroid. This implies that we learn $\mu_{g,c}$ for $g \in G, c \in \{1, \dots, C\}$ such that $\mu_{g,c}$ satisfies $\pi(g_1)^{-1}\mu_{g_1,c} = \pi(g_2)^{-1}\mu_{g_2,c}$ for all g_1, g_2, c . The algorithm is shown in Algorithm 2.

4.3. Invariant Feature Coding

We subsequently construct a feature coding function F as the \mathcal{G} -invariant vector in the space where \mathcal{G} acts orthogonally. We first use the space of the function of x_n where we can guarantee that \mathcal{G} acts orthogonally as the basis space, and construct more complex representation spaces using the tensor product. The first basis space is the space of x_n itself. The second is the $C|G|$ -dimensional 1-of-k vector that we assign x_n to the nearest $\mu_{g,c}$. When we apply $\pi(g)$ on x_n , the nearest μ corresponds to the vector where we apply $\pi(g)$ on the nearest $\mu_{g,c}$. Therefore, g acts as a permutation matrix on the space that is orthogonal. We denote this representation as $1_{\mu}(g)$.

Invariant Bilinear Pooling Since BP is written as the tensor product of x_n , we can directly use

$$F = \text{vec} \left(\frac{1}{N} \sum_{n=1}^N P_1(x_n \otimes x_n) \right), \quad (6)$$

as the invariant global feature. Though P_1 is a projection to the trivial representation defined by Eq. (1), we can calculate this feature from the irreducible decomposition of x_n and the irreducible decomposition of the tensor products. We can also apply normalization on the invariant covariance with respect to each $P_1(\tau_{t,o} \otimes \tau_{t,o})$ -th elements to get the variant of BP such as iBP. Because we discard elements that are not invariant, the feature dimensions of these methods are smaller than the original ones.

Invariant VLAD We subsequently propose an invariant version of the VLAD. The difficulty is first, at first sight, VLAD is not the form of the tensor product, and second, the effect of transformation on the nearest code word is not consistent. We solve the first difficulty by regarding VLAD as the tensor product of the local feature and 1-of-k representation, and the second difficulty by using Invariant k-means proposed in Section 4.2 to learn the code word.

The expression of Invariant VLAD is as follows:

$$F = \text{vec} \left(\frac{1}{N} \sum_{n=1}^N P_1(1_{\mu}(x_n) \otimes (x_n - \mu_c)) \right), \quad (7)$$

where μ_c is the nearest centroid to x_n . Because $1_{\mu}(x_n)$ is the vector where only the elements corresponding to the nearest μ is 1, the tensor product becomes the vector where the elements corresponding to the nearest μ is $x_n - \mu_c$, which is the same as the original VLAD. Because both $1_{\mu}(x_n)$ and $x_n - \mu_c$ are orthogonal representation spaces, this space is also an orthogonal representation space. Although the size of the codebook becomes $|G|$ -times larger, the dimensions of the global feature is not as large because we only use the invariant vector. When we use the D4 group, as will be described later, we can prove that the dimension of the Invariant VLAD is Cd_{local} .

Invariant VLAT We finally propose the invariant VLAT that can incorporate local second-order statistics. We can calculate the feature by combining the two features above.

$$F = \text{vec} \left(\frac{1}{N} \sum_{n=1}^N P_1(1_{\mu}(x_n) \otimes ((x_n - \mu_c) \otimes (x_n - \mu_c) - \mathcal{T}_c)) \right). \quad (8)$$

The dimension of the Invariant VLAT with $C|G|$ components is the same as that of the VLAT with C components.

Thus, we can model complex nonlinear statistics and calculate the invariants using the tensor product representation when we use local polynomial statistics as a global feature.

4.4. D4 group

In the experiment, we used the D4 group in [5] that contains rich information, and is easy to calculate. The D4 group is a group consisting of $\pi/2$ rotation r , and an image flipping m with $|G| = 8$. We summarize the property of the D4 group in the supplementary materials.

Because D4 does not act orthogonally to the output of general CNNs, we pretrained the group equivariant CNNs with respect to the D4 group and used the last convolutional activation as the local feature extractor. The group equivariant CNN is the model where we preserve the \mathcal{G} action using $|G|$ -times number of filters where we applied $\pi(g)$ on the original filters, and used the average with respect to g when

Table 1. Comparison of accuracy using fixed features.

Methods	Dim.	Test Accuracy					Augmented Test Accuracy				
		FMD	DTD	UIUC	CUB	Cars	FMD	DTD	UIUC	CUB	Cars
BP	525k	81.28	75.89	80.83	77.48	86.22	78.17	70.90	69.12	37.35	27.45
iBP	525k	81.38	75.88	81.94	75.90	86.74	78.28	71.00	69.39	38.32	28.45
VLAD	525k	80.38	75.12	80.37	72.94	86.10	77.20	70.62	67.95	36.18	29.78
VLAT	525k	79.98	76.24	80.46	76.62	87.12	77.03	71.45	69.87	41.01	27.27
FV	525k	78.18	75.56	79.35	66.59	81.70	75.28	70.78	65.89	29.36	27.37
Inv BP	82k	83.34	77.19	81.48	81.79	87.45	83.05	77.09	81.48	81.62	87.50
Inv iBP	82k	83.46	77.96	83.33	82.12	88.80	83.24	77.83	83.38	81.98	88.80
Inv VLAD	525k	82.42	76.53	81.94	80.97	88.54	82.15	76.38	81.68	80.75	88.54
Inv VLAT	525k	81.88	77.45	82.13	83.25	88.59	81.77	77.36	82.13	83.01	88.62

Table 2. Comparison of accuracy using the end-to-end model. The score with (reported)’’ denotes the score reported in the original paper [19]. Note that the reported score used non-equivariant Resnet.

Method	ResNet50			ResNet101		
	iSQRT-COV (reported) [19]	iSQRT-COV [19]	Inv iSQRT-COV	iSQRT-COV (reported) [19]	iSQRT-COV [19]	Inv iSQRT-COV
Dim.	32k	265k	25k	32k	265k	25k
Top-1 Err.	22.14	21.65	21.02	21.21	20.45	19.98
Top-5 Err.	6.22	5.92	5.47	5.68	5.35	4.96

we applied convolution. When the feature is a $d_{\text{CNN}} \times 8$ dimension, it can be regarded as d_{CNN} times the direct sum of the eight-dimensional orthogonal representation space because D4 acts as a permutation. The representation is decomposed as follows: $\pi_{\text{CNN}} = d_{\text{CNN}}\tau_{1,1} \oplus d_{\text{CNN}}\tau_{1,-1} \oplus d_{\text{CNN}}\tau_{-1,1} \oplus d_{\text{CNN}}\tau_{-1,-1} \oplus 2d_{\text{CNN}}\tau_2$.

5. Experiment

5.1. Experiment with fixed local features

In this subsection, we evaluated our methods on image recognition datasets using pretrained CNN local features. Note that we fixed the local features to compare only the performance of coding methods, and thus the overall scores are lower than the existing end-to-end methods.

We evaluated the methods on the Flickr Material Dataset (FMD) [32], describable texture datasets (DTD) [3], UIUC material dataset (UIUC) [20], Caltech-UCSD Birds (CUB) [39] and Stanford Cars (Cars) [17]. FMD contains 10 material categories with 1,000 images. DTD contains 47 texture categories with 5,640 images. UIUC contains 18 categories with 216 images. CUB contains 200 bird categories with 11,788 images. Cars consists of 196 car categories with 16,185 images. We used the given train-test splits for DTD, CUB, and Cars, and randomly split 10 times such that the sizes of the training and testing data are the same for each category for the FMD and UIUC.

We pretrained the group equivariant CNNs with the VGG19 architecture with convolutional filter sizes of 23, 45, 91, 181, 181 instead of 64, 128, 256, 512, 512 as the local feature extractor. Further, we added batch normalization layers for each convolution layer to accelerate the training speed. We trained the model with the ILSVRC2012

dataset [6]. We applied the standard data augmentation strategy and used the same learning setting as the original VGG-Network.

We extracted the last convolutional activation of this pretrained group equivariant VGG19 after rescaling the input images by 2^s , where $s = -3, -2.5, \dots, 1.5$. For efficiency, we discarded the scales that increased the image size to more than $1,024^2$ pixels. Subsequently, we applied the non-linear embedding proposed in [35] such that the feature dimension is three times as large. Because this embedding is a point-wise function, we can regard the output as three times the direct sum of the original representations when we consider the group action.

We subsequently reduce the local feature dimension using PCA for the existing method, and the proposed Invariant PCA for the proposed method. We applied BP and iBP with the dimension 1,024, VLAD with 512 dimension and 1,024 components, FV with 512 dimension and 512 components, and VLAT with 256 dimension and 8 components. We also applied the proposed BP and iBP with the same settings and VLAD and VLAT with eight times the number of components.

We used the linear SVM implemented in liblinear [8] and evaluated the average of the test accuracy. Further, to validate that the proposed feature is D4 invariant, we used the same training data and evaluated the accuracy when we augmented the test data eight times using the D4 group.

Table 1 shows the accuracy for the original test datasets and for the augmented test datasets. Our method demonstrates better accuracy than the non-invariant methods. Further, the dimensions of Invariant BP and iBP are approximately 1/7 the original dimensions. Thus, we obtained features with much smaller dimensions with higher per-

Table 3. Comparison of accuracy using fine-tuning. The score with (reported)” denotes the score reported in the original paper [19]. Note that the reported score used non-equivariant Resnet.

Method	ResNet50			ResNet101		
	iSQRT-COV (reported) [19]	iSQRT-COV[19]	Inv iSQRT-COV	iSQRT-COV (reported) [19]	iSQRT-COV[19]	Inv iSQRT-COV
Dim.	32k	265k	25k	32k	265k	25k
CUB	88.1	87.8	87.9	88.7	44.7	88.5
Cars	92.8	93.8	93.4	93.3	56.0	93.9
Aircraft	90.0	91.4	91.7	91.4	69.1	92.1

formance. Note that the higher accuracy is not the simple effect of dimensionality reduction, because in general, the accuracy becomes lower as the dimension becomes small. We observed that iBP with 400 local feature dimensions (80k global feature dimensions) shows 81.76 on FMD and 81.30 on UIUC. Furthermore, compact bilinear pooling with 82k feature dimension shows 81.54 on FMD and 79.81 on UIUC. Therefore the result is significant because Inv iBP shows better accuracy **in spite of** the lower feature dimension.

This table also shows that the existing methods show poor performance on the augmented test data, but the proposed methods demonstrate a similar performance to the original score. These results suggest that the existing methods use information that does not relate to image contents, but to some dataset biases such as the angle of contents in the image. Our method can discard such bias and focus on the contents of the image.

We report the results of further ablation study, comparison with data augmentation and results for the different local features in the supplementary materials.

5.2. Experiment with end-to-end model

We then applied our Invariant BP to the end-to-end learning framework and evaluated the accuracy on the ILSVRC2012 [6] dataset. We constructed the model based on the iSQRT-COV [19], which is the variant of BP that demonstrated good performance.

We used the group equivariant CNNs with Resnet50 and 101 [12] architecture as a local feature extractor, where we reduced the filter sizes as in the case of VGG19. We then substituted global average pooling with iSQRT-COV and proposed Invariant iSQRT-COV.

We learn the whole models, including feature extractor using a momentum grad with an initial learning rate 0.1, momentum 0.9, and weight decay rate to 1e-4 for 65 epochs with batch size 160. We multiplied the learning rate by 0.1 at 30, 45 and 60 epochs. We then evaluated the top-1 and top-5 test error. We used the average score for the original image and the flipped image for the evaluation.

Table 2 shows that though iSQRT-COV also gains accuracy by using local features extracted from equivariant CNN, our Inv iSQRT-COV demonstrates better accuracy with small feature dimension.

We further fine-tuned the above pretrained models and evaluated the accuracy on standard fine-grained recognition datasets: CUB, Cars, and Aircraft [23]. The Aircraft dataset consists of 100 categories with 6,667 training images and 3,333 test images. Following the settings of the existing studies, we resized each input image to 448 x 448 for fine-tuning and evaluation for CUB and Cars, and we resized the images to 512 x 512 and cropped the 448 x 448 center image for the Aircraft dataset. Following the original setting of iSQRT-COV [19], we set the batch size as 10 and the weight decay rate as 1e-3 and trained the model with momentum grad with learning rates of 1.2e-3 for the feature extractor and 6e-3 for the classifier. We trained the model for 100 epochs. For each setting, we evaluated the models ten times and evaluated the average of the test accuracy.

Table 3 shows the results. As for ResNet50, the proposed Inv iSQRT-COV shows comparable or better accuracy than reported iSQRT-COV and similar accuracy to iSQRT-COV with equivariant ResNet50 with much smaller feature dimension. Furthermore, iSQRT-COV with equivariant ResNet101 overfits the training data and shows much lower accuracy than the proposed Inv iSQRT-COV ResNet101. This result suggests that our invariant feature coding contributes to the stability of the gradient-based training and results in exploiting complex local feature extractor and in high recognition accuracy.

Therefore, considering invariant feature coding is also effective for end-to-end training.

6. Conclusion

In this research, we proposed a feature coding method that considered the transformations that preserved the image information. Based on the group representation theory, we proposed a guideline that we first constructed a feature space in which a group acted orthogonally, and subsequently calculated the invariant vector. We subsequently constructed a novel model learning method and coding methods that explicitly considered group action. We applied our methods on image classification datasets and demonstrated that our model can yield high accuracy while preserving invariance. Our work becomes a novel framework when we construct an invariant feature.

Acknowledgements

This work was partially supported by JST CREST Grant Number JPMJCR1403, Japan, and partially supported by JSPS KAKENHI Grant Number JP19176033. We would like to thank Atsushi Kanehira, Takuhiro Kaneko, Toshihiko Matsuura, Takuya Nanri and Masatoshi Hidaka for the helpful discussion.

References

- [1] Fabio Anselmi, Joel Z Leibo, Lorenzo Rosasco, Jim Mutch, Andrea Tacchetti, and Tomaso Poggio. Unsupervised learning of invariant representations. *Theoretical Computer Science*, 633:112–121, 2016. 2
- [2] Relja Arandjelovic, Petr Gronat, Akihiko Torii, Tomas Pajdla, and Josef Sivic. Netvlad: Cnn architecture for weakly supervised place recognition. In *CVPR*, 2016. 1
- [3] Mircea Cimpoi, Subhransu Maji, Iasonas Kokkinos, Sammy Mohamed, and Andrea Vedaldi. Describing textures in the wild. In *CVPR*, 2014. 7, 13
- [4] Taco Cohen and Max Welling. Group equivariant convolutional networks. In *ICML*, 2016. 1, 2
- [5] Taco S Cohen and Max Welling. Steerable cnns. In *ICLR*, 2017. 1, 6
- [6] J. Deng, W. Dong, R. Socher, L.-J. Li, K. Li, and L. Fei-Fei. ImageNet: A Large-Scale Hierarchical Image Database. In *CVPR*, 2009. 7, 8, 13
- [7] Mandar D Dixit and Nuno Vasconcelos. Object based scene representations using fisher scores of local subspace projections. In *NeurIPS*, 2016. 2
- [8] Rong-En Fan, Kai-Wei Chang, Cho-Jui Hsieh, Xiang-Rui Wang, and Chih-Jen Lin. LIBLINEAR: A library for large linear classification. *JMLR*, 9:1871–1874, 2008. 7
- [9] William Fulton and Joe Harris. *Representation Theory: A First Course*. Springer, 2014. 3
- [10] Yang Gao, Oscar Beijbom, Ning Zhang, and Trevor Darrell. Compact bilinear pooling. In *CVPR*, 2016. 1
- [11] Mengran Gou, Fei Xiong, Octavia Camps, and Mario Sznaier. Monet: Moments embedding network. In *CVPR*, 2018. 2
- [12] Kaiming He, Xiangyu Zhang, Shaoqing Ren, and Jian Sun. Deep residual learning for image recognition. In *CVPR*, 2016. 8
- [13] Emiel Hoogeboom, Jorn W.T. Peters, Taco S. Cohen, and Max Welling. Hexaconv. In *ICLR*, 2018. 13
- [14] Hervé Jégou, Matthijs Douze, Cordelia Schmid, and Patrick Pérez. Aggregating local descriptors into a compact image representation. In *CVPR*, 2010. 2
- [15] Takumi Kobayashi. Flip-invariant motion representation. In *ICCV*, 2017. 3
- [16] Takumi Kobayashi, Koiti Hasida, and Nobuyuki Otsu. Rotation invariant feature extraction from 3-d acceleration signals. In *ICASSP*, 2011. 2
- [17] Jonathan Krause, Michael Stark, Jia Deng, and Li Fei-Fei. 3d object representations for fine-grained categorization. In *ICCV*, 2013. 7
- [18] Dmitry Laptev, Nikolay Savinov, Joachim M Buhmann, and Marc Pollefeys. Ti-pooling: transformation-invariant pooling for feature learning in convolutional neural networks. In *CVPR*, 2016. 2
- [19] Peihua Li, Jiangtao Xie, Qilong Wang, and Zilin Gao. Towards faster training of global covariance pooling networks by iterative matrix square root normalization. In *CVPR*, 2018. 7, 8
- [20] Zicheng Liao, Jason Rock, Yang Wang, and David Forsyth. Non-parametric filtering for geometric detail extraction and material representation. In *CVPR*, 2013. 7, 13
- [21] Tsung-Yu Lin and Subhransu Maji. Improved bilinear pooling with cnns. In *BMVC*, 2017. 2
- [22] Tsung-Yu Lin, Aruni RoyChowdhury, and Subhransu Maji. Bilinear cnn models for fine-grained visual recognition. In *ICCV*, 2015. 1, 2
- [23] S. Maji, J. Kannala, E. Rahtu, M. Blaschko, and A. Vedaldi. Fine-grained visual classification of aircraft. Technical report, 2013. 8
- [24] Diego Marcos, Michele Volpi, Nikos Komodakis, and Devis Tuia. Rotation equivariant vector field networks. In *ICCV*, 2017. 2
- [25] Olivier Morère, Antoine Veillard, Lin Jie, Julie Petta, Vijay Chandrasekhar, and Tomaso Poggio. Group invariant deep representations for image instance retrieval. In *AAAI*, 2017. 3
- [26] Hideki Nakayama, Tatsuya Harada, and Yasuo Kuniyoshi. Dense sampling low-level statistics of local features. *IEICE TRANSACTIONS on Information and Systems*, 93:1727–1736, 2010. 2
- [27] Hideki Nakayama, Tatsuya Harada, and Yasuo Kuniyoshi. Global gaussian approach for scene categorization using information geometry. In *CVPR*, 2010. 2
- [28] David Picard and Philippe-Henri Gosselin. Efficient image signatures and similarities using tensor products of local descriptors. *CVIU*, 117:680–687, 2013. 2
- [29] Marco Reiser and Hans Burkhardt. Using irreducible group representations for invariant 3d shape description. In *Joint Pattern Recognition Symposium*, 2006. 2
- [30] Jongbin Ryu, Ming-Hsuan Yang, and Jongwoo Lim. Dft-based transformation invariant pooling layer for visual classification. In *ECCV*, 2018. 3
- [31] Jorge Sánchez, Florent Perronnin, Thomas Mensink, and Jakob Verbeek. Image classification with the fisher vector: Theory and practice. *IJCV*, 105:222–245, 2013. 1, 2
- [32] Lavanya Sharan, Ce Liu, Ruth Rosenholtz, and Edward H Adelson. Recognizing materials using perceptually inspired features. *IJCV*, 103(3):348–371, 2013. 7, 13
- [33] Karen Simonyan and Andrew Zisserman. Very deep convolutional networks for large-scale image recognition. In *ICLR*, 2014. 1
- [34] Jure Sokolic, Raja Giryes, Guillermo Sapiro, and Miguel RD Rodrigues. Generalization error of invariant classifiers. In *AISTATS*, 2017. 5
- [35] Andrea Vedaldi and Andrew Zisserman. Efficient additive kernels via explicit feature maps. *PAMI*, 34(3):480–492, 2012. 7, 13

- [36] Qilong Wang, Peihua Li, and Lei Zhang. G2denet: Global gaussian distribution embedding network and its application to visual recognition. In *CVPR, 2017*. 2
- [37] Qilong Wang, Peihua Li, Wangmeng Zuo, and Lei Zhang. Raid-g: Robust estimation of approximate infinite dimensional gaussian with application to material recognition. In *CVPR, 2016*. 1
- [38] Maurice Weiler, Fred A Hamprecht, and Martin Storath. Learning steerable filters for rotation equivariant cnns. In *CVPR, 2018*. 2
- [39] Peter Welinder, Steve Branson, Takeshi Mita, Catherine Wah, Florian Schroff, Serge Belongie, and Pietro Perona. Caltech-ucsd birds 200. Technical Report CNS-TR-201, Caltech, 2010. 7, 13
- [40] Daniel E Worrall, Stephan J Garbin, Daniyar Turmukhambetov, and Gabriel J Brostow. Harmonic networks: Deep translation and rotation equivariance. In *CVPR, 2017*. 1, 2

A. Illustrative Example of the proposed method.

We visualize our methods in the simple setting.

Group consists of identity mapping and image flipping.

We consider the group consists of identity mapping e and horizontal image flipping m . Since we get the original image by applying image flipping twice, it follows that $e \circ e = e$, $e \circ m = m$, $m \circ e = m$, $m \circ m = e$. This definition satisfies the three properties of a group by setting $m^{-1} = m$:

- \circ is associative: $g_1, g_2, g_3 \in G$ satisfies $((g_1 \circ g_2) \circ g_3) = (g_1 \circ (g_2 \circ g_3))$.
- The identity element $e \in G$ exists that satisfies $g \circ e = e \circ g = g$ for all $g \in G$.
- All $g \in G$ contains the inverse g^{-1} that satisfies $g \circ g^{-1} = g^{-1} \circ g = e$.

Also, we can see that the irreducible representations are $\tau_1 : \tau_1(e) = 1, \tau_1(m) = 1$ and $\tau_{-1} : \tau_{-1}(e) = 1, \tau_{-1}(m) = -1$. This is proved as follows: The τ s defined above satisfy the conditions of representation

- For $g_1, g_2 \in G$, $\tau(g_1) \circ \tau(g_2) = \tau(g_1 \circ g_2)$.
- $\tau(e) = 1_{d \times d}$.

1-dimensional representations are trivially irreducible. When the dimension of the representation space is larger than 1, we denote $\pi(e) = 1_{d \times d}$ and $\pi(m) = A \in \text{GL}(d, \mathbb{C})$. We apply eigendecomposition of A to obtain $A = T^{-1}\Lambda T$ where Λ is diagonal and we denote the i -th diagonal elements as λ_i . Because $\pi(e) = T^{-1}1_{d \times d}T$ and $\pi(m) = T^{-1}\Lambda T$, this implies π is decomposed as a direct sum representation of $\pi_i(e) = 1, \pi_i(m) = \lambda_i$ for each i -th dimension. Therefore, this representation is not irreducible. Thus the irreducible representation needs to be

1-dimensional. Also, $\pi(m)^2 = \pi(e) = 1$. Thus, $\pi(m)$ is 1 or -1.

Image feature and its irreducible decomposition.

As an image feature, we use the concatenation of luminosity of two horizontally adjacent pixels as a local feature and apply average pooling to get a global feature. Thus, the feature dimension is 2. Since image flipping changes the order of the pixels, it acts as the permutation of first and second elements in the feature space. Therefore, the group acts as $\pi(e) = \begin{pmatrix} 1 & 0 \\ 0 & 1 \end{pmatrix}$, $\pi(m) = \begin{pmatrix} 0 & 1 \\ 1 & 0 \end{pmatrix}$, as plotted in the left figure of Figure 2. By applying orthogonal matrices calculated by Eq. (7) in the original paper, we get the feature space written in the center of Figure 2. In this space, the group acts as $\pi(e) = \begin{pmatrix} 1 & 0 \\ 0 & 1 \end{pmatrix}$, $\pi(m) = \begin{pmatrix} 1 & 0 \\ 0 & -1 \end{pmatrix}$. Thus, this is the irreducible decomposition of π into $\tau_1 \oplus \tau_{-1}$ defined by the **Irreducible representation** paragraph in Section 3 of the original paper. **Note that in the general case, each representation matrix is block-diagonalized instead of diagonalized and each diagonal block becomes more complex, like those written in Table 1 in the original paper.**

Invariant classifier.

In this decomposed space, when we train the classifier by considering both original images and flipped images, the classification boundary learned with l2-regularized convex loss minimization becomes the form of $x = b$ as plotted in the right figure of Figure 2. Thus, we can discard y -elements of features and get a compact feature vector. This result is validated as follows: when we denote the feature in the decomposed space that corresponds to the original image as (x_n, y_n) , the feature corresponds to the flipped image becomes $(x_n, -y_n)$ because $\pi(m) = \begin{pmatrix} 1 & 0 \\ 0 & -1 \end{pmatrix}$. When we write the linear classifier as $w_x^t x + w_y^t y + w_b$, the loss for these two images are written as $l(w_x^t x_n + w_y^t y_n + b) + l(w_x^t x_n - w_y^t y_n + b)$. From Jensen's inequality, this is lower-bounded by $2l(w_x^t x_n + b)$. This means that the loss is minimized when $w_y = 0$, resulting in the classification boundary $w_x^t x + w_b = 0$. This calculation is generalized to Eq. (10) in the original paper.

Tensor product representation.

Subsequently, we consider the 'product' of feature space to get nonlinear features. We consider the two feature spaces (x^1, y^1) and (x^2, y^2) with π acts as $\pi(e) = \begin{pmatrix} 1 & 0 \\ 0 & 1 \end{pmatrix}$, $\pi(m) = \begin{pmatrix} 0 & 1 \\ 1 & 0 \end{pmatrix}$ on both spaces. We can use any input spaces whenever these spaces and π satisfy the above condition. For example, we use the same feature space for (x^1, y^1) and (x^2, y^2) to obtain bilinear pooling. The tensor product of these spaces becomes a 4-dimensional vector space consisting of

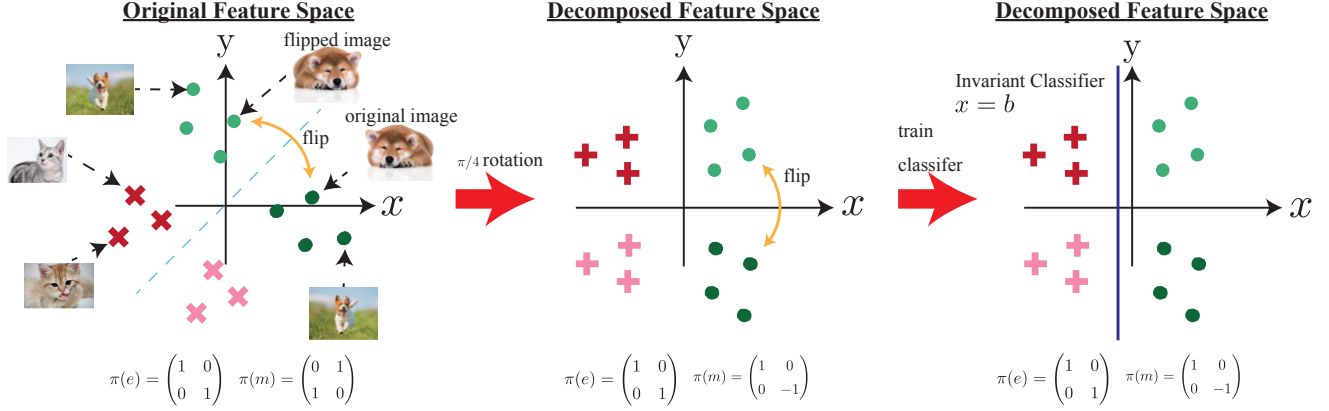


Figure 2. Example of the irreducible decomposition and learned classifier.

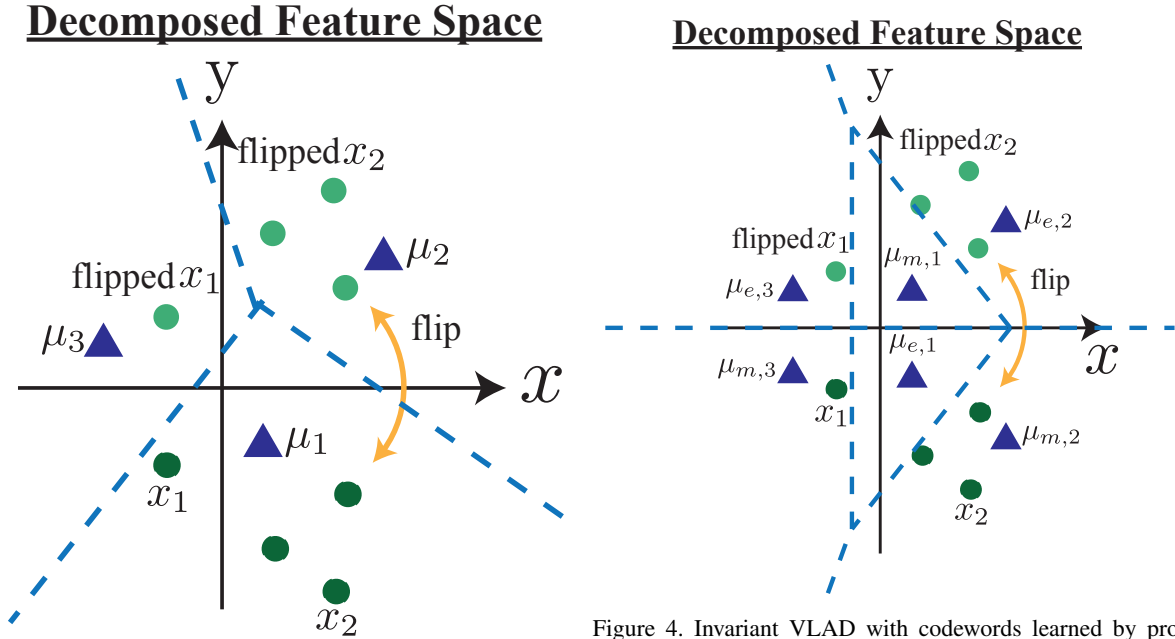


Figure 3. VLAD with codewords learned by k-means.

Figure 4. Invariant VLAD with codewords learned by proposed k-means.

$x^1x^2, x^1y^2, y^1x^2, y^1y^2$. Since m acts as permutations of x^1 and y^1 , x^2 and y^2 at the same time, m acts as permutations of x^1x^2 and y^1y^2 and x^1y^2 and y^1x^2 at the same

time. Thus, $\pi(m)$ is written as $\pi(m) = \begin{pmatrix} 0 & 0 & 0 & 1 \\ 0 & 0 & 1 & 0 \\ 0 & 1 & 0 & 0 \\ 1 & 0 & 0 & 0 \end{pmatrix}$.

Thus, tensor product space is also the group representation space. This space can also be decomposed into irre-

ducible representations as $\pi(e) = \begin{pmatrix} 1 & 0 & 0 & 0 \\ 0 & 1 & 0 & 0 \\ 0 & 0 & 1 & 0 \\ 0 & 0 & 0 & 1 \end{pmatrix}$ and

$\pi(m) = \begin{pmatrix} 1 & 0 & 0 & 0 \\ 0 & 1 & 0 & 0 \\ 0 & 0 & -1 & 0 \\ 0 & 0 & 0 & -1 \end{pmatrix}$. We only need the first 2 elements as an invariant feature.

Invariant k-means and VLAD. As plotted in Figure 3, when the learned codebook is μ_i for $i = 1, 2, 3$, x_1 and x_2 are both assigned to μ_1 . When these features are flipped, flipped x_1 is assigned to μ_3 while flipped x_2 is assigned to μ_2 . Thus, image flipping does not act consistently on the assignment vector $1_\mu(x_n)$. As plotted in Figure 4, when we learn the codebook so that there exists μ with y -element flipped for each codeword, the group acts consistently on

$1_\mu(x_n)$. It is because whenever x_n is assigned to $\mu_{e,i}$, flipped x_n is assigned to $\mu_{m,i}$. Also flipped x_n is assigned to $\mu_{e,i}$ when x_n is assigned to $\mu_{m,i}$. Thus, the group acts orthogonally on $1_\mu(x_n)$.

B. Invariant PCA when the irreducible representations are not real.

In the case where some τ have complex elements, we cannot apply Algorithm 1 directly because the intertwining operator and covariance matrices become complex. In this case, we couple τ_t with $\bar{\tau}_t$ into $\tau' \simeq \tau_t \oplus \bar{\tau}_t$. Because $\chi_{\bar{\tau}_t} = \overline{\chi_{\tau_t}}$, the multiplicity of τ_t and $\bar{\tau}_t$ in the decomposition are equal because of Eq. (6), and the projected vectors are complex conjugates of each other because of (7). Thus, $\sqrt{2}$ times the concatenation of the real and imaginary parts becomes the τ' -th elements. We replace τ_t with τ'_t defined above in Algorithm 1 to obtain Invariant PCA in the general case.

C. Property of D4 group

We summarize the irreducible representations and decomposition of the tensor products in Tables 4 and 5 respectively.

D. Proof that the dimension of Invariant VLAD and VLAT is the same as that of original feature

When we use C components, we can decompose 1_μ into $C\tau_{1,1} \oplus C\tau_{1,-1} \oplus C\tau_{-1,1} \oplus C\tau_{-1,-1} \oplus 2C\tau_2$. When first or second order statistics are decomposed as $n_{1,1}\tau_{1,1} \oplus n_{1,-1}\tau_{1,-1} \oplus n_{-1,1}\tau_{-1,1} \oplus n_{-1,-1}\tau_{-1,-1} \oplus n_2\tau_2$, the multiplicity of $\tau_{1,1}$ of $(C\tau_{1,1} \oplus C\tau_{1,-1} \oplus C\tau_{-1,1} \oplus C\tau_{-1,-1} \oplus 2C\tau_2) \otimes (n_{1,1}\tau_{1,1} \oplus n_{1,-1}\tau_{1,-1} \oplus n_{-1,1}\tau_{-1,1} \oplus n_{-1,-1}\tau_{-1,-1} \oplus n_2\tau_2)$ is $C(n_{1,1} + n_{1,-1} + n_{-1,1} + n_{-1,-1} + 2n_2)$, which is the same as the dimension of original feature.

E. Results using only proposed feature modeling

As an ablation study, we conducted the experiments that we trained the PCA and k-means using proposed invariant feature modeling and then applied existing feature coding methods.

Table 6 demonstrates that the proposed invariant feature modeling combined with the standard feature coding method does not demonstrate better accuracy than the original methods. This result shows that we gain performance only when we combine the proposed invariant feature modeling and invariant feature coding.

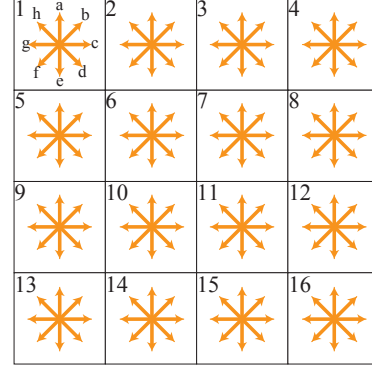


Figure 5. Overview of the SIFT feature.

F. Results using data augmentation

We also compared our results with data augmentation. We trained existing non-invariant feature coding with 8 times data augmentation. Due to the much larger training cost, we conducted experiments on the FMD and UIUC datasets.

Table 7 shows that the accuracy is comparable or a little lower than the accuracy of the proposed invariant feature coding methods. This result is consistent with the argument of Theorem 1 that invariant features learned with the original training data is equivalent to non-invariant features learned with the augmented training data. Therefore, our methods exploit the advantage of data augmentation with lower feature dimensions and lower training costs.

G. Results on SIFT features

In this section, we report the results using the SIFT feature that D4 acts orthogonally. We describe the irreducible decomposition of the SIFT feature in Section G.1. We evaluate the accuracy on image recognition datasets in Section G.2.

G.1. Irreducible decomposition of SIFT

We plot the overview of the SIFT feature in Figure 5, where a D4 group acts as a permutation on both $\{a, b, c, d, e, f, g, h\}$ and $1..16$. We can further decompose these into permutations on $\{a, c, e, g\}$, $\{b, d, f, h\}$, $\{1, 4, 13, 16\}$, $\{6, 7, 10, 11\}$, and $\{2, 3, 5, 8, 9, 12, 13, 14\}$. These permutations can be decomposed as $\tau_{1,1} \oplus \tau_{-1,1} \oplus \tau_2$, $\tau_{1,1} \oplus \tau_{-1,-1} \oplus \tau_2$, $\tau_{1,1} \oplus \tau_{-1,-1} \oplus \tau_2$, $\tau_{1,1} \oplus \tau_{-1,-1} \oplus \tau_2$, and $\tau_{1,1} \oplus \tau_{-1,1} \oplus \tau_{1,-1} \oplus \tau_{-1,-1} \oplus \tau_2$ respectively, which can be calculated using characteristic functions. Thus, permutations on SIFT can be decomposed as $(2\tau_{1,1} \oplus \tau_{-1,1} \oplus \tau_{-1,-1} \oplus 2\tau_2) \otimes (3\tau_{1,1} \oplus \tau_{1,-1} \oplus \tau_{-1,1} \oplus 3\tau_{-1,-1} \oplus 4\tau_2) = 18\tau_{1,1} \oplus 14\tau_{1,-1} \oplus 14\tau_{-1,1} \oplus 18\tau_{-1,-1} \oplus 32\tau_2$.

Table 4. Irreducible representations of the D4 group.

Rep.	e	r	r^2	r^3	m	mr	mr^2	mr^3
$\tau_{1,1}$	1	1	1	1	1	1	1	1
$\tau_{1,-1}$	1	1	1	1	-1	-1	-1	-1
$\tau_{-1,1}$	1	-1	1	-1	1	-1	1	-1
$\tau_{-1,-1}$	1	-1	1	-1	-1	1	-1	1
τ_2	$\begin{bmatrix} 1 & 0 \\ 0 & 1 \end{bmatrix}$	$\begin{bmatrix} 0 & -1 \\ 1 & 0 \end{bmatrix}$	$\begin{bmatrix} -1 & 0 \\ 0 & -1 \end{bmatrix}$	$\begin{bmatrix} 0 & 1 \\ -1 & 0 \end{bmatrix}$	$\begin{bmatrix} -1 & 0 \\ 0 & 1 \end{bmatrix}$	$\begin{bmatrix} 0 & 1 \\ 1 & 0 \end{bmatrix}$	$\begin{bmatrix} 1 & 0 \\ 0 & -1 \end{bmatrix}$	$\begin{bmatrix} 0 & -1 \\ -1 & 0 \end{bmatrix}$

Table 5. Irreducible representations of tensor products of irreducible representations of the D4 group.

	$\tau_{1,1}$	$\tau_{1,-1}$	$\tau_{-1,1}$	$\tau_{-1,-1}$	τ_2
$\tau_{1,1}$	$\tau_{1,1}$	$\tau_{1,-1}$	$\tau_{-1,1}$	$\tau_{-1,-1}$	τ_2
$\tau_{1,-1}$	$\tau_{1,-1}$	$\tau_{1,1}$	$\tau_{-1,-1}$	$\tau_{-1,1}$	τ_2
$\tau_{-1,1}$	$\tau_{-1,-1}$	$\tau_{-1,1}$	$\tau_{1,-1}$	$\tau_{1,1}$	τ_2
$\tau_{-1,-1}$	$\tau_{-1,-1}$	$\tau_{-1,1}$	$\tau_{1,-1}$	$\tau_{1,1}$	τ_2
τ_2	τ_2	τ_2	τ_2	τ_2	$\tau_{1,1} \oplus \tau_{1,-1} \oplus \tau_{-1,1} \oplus \tau_{-1,-1}$

G.2. Experimental Results

We evaluated the methods on (FMD) [32], (DTD) [3], (UIUC) [20] and CUB [39]). The evaluation protocol is the same as that of the VGG-feature.

We extracted the dense SIFT feature from multi-scale images like the case of VGG, then applied nonlinear homogeneous mapping [35] to make the feature dimension three times as large.

We reduced the dimension to 256, and then we applied BP, VLAD with 1,024 components, FV with 512 components, and VLAT with 16 components. We also applied the proposed Invariant BP with the same setting and VLAD and VLAT with eight times the number of components.

Table 8 shows a similar tendency as the results for the VGG-feature. Our methods demonstrate better performance than existing methods for both original test data and augmented test data.

H. Application to D6 group

Furthermore, we apply our method to the D6 group that is more complex than the D4 group. The D6 group consists of $\pi/3$ rotation r and an image flipping m with $|G| = 12$. We summarize the irreducible representations and decomposition of the tensor products for this group in Tables 9 and 10 respectively.

To obtain the local feature that D6 acts orthogonally, we pretrained the CNN with hexaconv [13]. Hexaconv models the input images in the hexagonal axis and applies D6 group-equivariant convolutional layers to construct the CNN. Since D6 acts as a permutation of the positions in this hexagonal axis, the convolutional activations are D6-equivariant. Therefore, we can use this convolutional activation as the input for our coding methods.

We pretrained the group equivariant CNNs with the VGG19 architecture with convolutional filter sizes of 18, 37, 74, 148, 148 instead of 64, 128, 256, 512, 512 as the

local feature extractor. Further, we added batch normalization layers for each convolution layer to accelerate the training speed. Therefore, the dimensionality of the local features is 148×12 . We trained the model with the ILSVRC2012 dataset [6]. Since the input image size increases when we change the axes from Euclidean to hexagonal, we randomly cropped a 160×160 image from the original image rescaled to 192×192 for training. The rest of the settings followed the original VGG.

We extracted the last convolutional activation of this pretrained model after rescaling the input images by 2^s , where $s = -3, -2.5, \dots, 1.5$. For efficiency, we discarded the scales that increased the image size to more than 512^2 pixels. Subsequently, we applied the nonlinear embedding proposed in [35]. The dimension and the number of components used for the coding methods followed those for the D4 experiments.

We can see from Table 11 that though the overall accuracy is lower than the D4 case, which may arise from the discriminative performance of the local feature extractor itself, the proposed coding methods consistently demonstrate better performance than the non-invariant methods. Furthermore, the dimensionality of Invariant BP and iBP is smaller than the dimensionality for the D4 case. This is because the D6 group represents more complex transformations than the D4 group, and thus the number of invariants with respect to the D6 group is smaller than the number with respect to the D4 group.

Therefore, the proposed framework is also effective for the D6 group.

Table 6. Comparison of accuracy using invariant feature modeling and existing feature coding methods.

Methods	Dim.	FMD	DTD	UIUC	CUB	Cars
BP	525k	81.20	75.09	80.19	78.24	85.67
iBP	525k	81.20	75.05	81.20	76.36	86.00
VLAD	525k	80.50	75.20	78.80	71.61	85.72
VLAT	525k	79.98	75.66	81.02	78.29	84.77
FV	525k	78.50	75.63	79.91	67.47	82.47

Table 7. Comparison of accuracy using existing feature coding methods with augmented training data.

Methods	Dim.	FMD	UIUC
BP	525k	83.00	81.11
iBP	525k	83.10	82.87
VLAD	525k	82.72	80.56
VLAT	525k	82.66	81.67
FV	525k	81.44	80.74

Table 8. Comparison of accuracy using SIFT features.

Methods	Dim.	Test Accuracy			Augmented Test Accuracy		
		FMD	DTD	UIUC	FMD	DTD	UIUC
BP	33k	49.84	51.54	56.02	43.36	41.55	42.50
VLAD	262k	60.11	59.37	58.70	54.68	51.54	46.11
VLAT	525k	58.09	58.74	59.72	52.01	50.40	47.85
FV	262k	61.84	61.20	64.26	56.78	53.77	51.89
Inv BP	8k	55.19	54.78	60.74	55.18	54.79	60.74
Inv VLAD	262k	67.53	64.50	68.98	67.55	64.53	69.04
Inv VLAT	525k	66.79	64.60	67.50	66.75	64.61	67.57

Table 9. Irreducible representations of the D6 group.

Rep.	r	m
$\tau_{1,1}$	1	1
$\tau_{1,-1}$	1	-1
$\tau_{-1,1}$	-1	1
$\tau_{-1,-1}$	-1	-1
τ_{2a}	$\begin{bmatrix} \cos(\pi/3) & -\sin(\pi/3) \\ \sin(\pi/3) & \cos(\pi/3) \end{bmatrix}$	$\begin{bmatrix} 0 & -1 \\ 1 & 0 \end{bmatrix}$
τ_{2b}	$\begin{bmatrix} \cos(2\pi/3) & -\sin(2\pi/3) \\ \sin(2\pi/3) & \cos(2\pi/3) \end{bmatrix}$	$\begin{bmatrix} 0 & -1 \\ 1 & 0 \end{bmatrix}$

Table 10. Irreducible representations of the tensor products of irreducible representations of the D6 group.

	$\tau_{1,1}$	$\tau_{1,-1}$	$\tau_{-1,1}$	$\tau_{-1,-1}$	τ_{2a}	τ_{2b}
$\tau_{1,1}$	$\tau_{1,1}$	$\tau_{1,-1}$	$\tau_{-1,1}$	$\tau_{-1,-1}$	τ_{2a}	τ_{2b}
$\tau_{1,-1}$	$\tau_{1,-1}$	$\tau_{1,1}$	$\tau_{-1,-1}$	$\tau_{-1,1}$	τ_{2a}	τ_{2b}
$\tau_{-1,1}$	$\tau_{-1,-1}$	$\tau_{-1,1}$	$\tau_{1,-1}$	$\tau_{1,1}$	τ_{2b}	τ_{2a}
$\tau_{-1,-1}$	$\tau_{-1,-1}$	$\tau_{-1,1}$	$\tau_{1,-1}$	$\tau_{1,1}$	τ_{2b}	τ_{2a}
τ_{2a}	τ_{2a}	τ_{2a}	τ_{2b}	τ_{2b}	$\tau_{1,1} \oplus \tau_{1,-1} \oplus \tau_{2b}$	$\tau_{-1,1} \oplus \tau_{-1,-1} \oplus \tau_{2a}$
τ_{2b}	τ_{2b}	τ_{2b}	τ_{2a}	τ_{2a}	$\tau_{-1,1} \oplus \tau_{-1,-1} \oplus \tau_{2a}$	$\tau_{1,1} \oplus \tau_{1,-1} \oplus \tau_{2b}$

Table 11. Comparison of test accuracy using D6-equivariant CNN.

Methods	Dim.	FMD	DTD	UIUC	CUB	Cars
BP	525k	77.26	73.46	75.93	72.66	80.15
iBP	525k	77.18	73.51	75.56	71.19	81.13
VLAD	525k	75.80	71.65	70.19	64.69	78.44
VLAT	525k	75.70	72.60	72.31	69.92	78.59
FV	525k	75.24	72.37	74.91	63.06	75.55
Inv BP	55k	80.26	75.41	79.26	78.77	80.92
Inv iBP	55k	80.36	75.86	80.09	79.74	83.60
Inv VLAD	525k	78.00	72.76	73.98	76.12	82.47
Inv VLAT	525k	78.06	74.15	75.65	77.59	80.15